D. S. Sankar*, Usik Lee and Ahmad Izani Md. Ismail

# Mathematical Analysis for MHD Flow of Blood in Constricted Arteries

**Abstract:** The unsteady oscillatory magneto-hydrodynamic flow of blood in small diameter arteries with mild constriction is analyzed, blood being modelled as a Herschel-Bulkley fluid. Finite difference method is employed for solving the associated initial boundary value problem. Explicit finite difference schemes for velocity distribution, flow rate, skin friction and longitudinal impedance to the flow are obtained. The effects of pressure gradient, yield stress, magnetic field, power law index and maximum depth of the stenosis on the aforesaid flow quantities are discussed through appropriate graphs. It is found that the velocity and flow rate decrease and the skin friction and longitudinal impedance to flow increase with the increase of the magnetic field parameter. It was recorded that the flow rate increases and the skin friction decreases with the increase of the phase angle. It was also noted the skin friction and longitudinal impedance to flow that increase almost linearly with the increase of maximum depth of the stenosis. The estimates of the increase in the longitudinal impedance to flow and skin friction are increased considerably by the presence of the magnetic field.

**Keywords:** hemodynamics, non-Newtonian fluids, constricted artery, MHD flow, FDM analysis

**PACS® (2010).** 35Q92, 76Z05

***Corresponding author: D. S. Sankar:** Division of Mathematics, School of Advanced Sciences, VIT University, Chennai 600127, India
E-mail: sankar_ds@yahoo.co.in
**Usik Lee:** Department of Mechanical Engineering, Inha University, Nam-Gu, Incheon 402751, Republic of Korea
**Ahmad Izani Md. Ismail:** School of Mathematical Sciences, Universiti Sains Malaysia, Penang 11800, Malaysia

## 1 Introduction

Atherosclerosis is an obstruction developed in the lumen of the artery due to the deposit of calcium, fat, cholesterol, cellular waste and fibrin [1–2]. Once an obstruction develops in the inner wall of the artery, the passage of the blood circulation is constricted and it results in stenosed artery [3, 4]. Since, the stenosis present in an artery leads to reduction in blood supply to the downstream; it increases the resistance to blood flow significantly and causes circulatory disorders [5, 6]. Stenoses formed in the cerebral arteries lead to strokes and the stenoses developed in the coronary arteries influences heart failure [7, 8]. It has been reported that the fluid dynamical properties of blood flow in the arteries with variable cross-section plays a vital role in the basic understanding and treatment of many cardiovascular diseases [9, 10]. Hence, the mathematical analysis of blood flow in constricted arteries is very useful.

Due to the complex interaction of the intercellular protein, blood behaves like a magnetic fluid and its magnetic properties are affected by the state of oxygenation [11]. The magnetohydrodynamic (MHD) flow of blood in arteries has many clinical applications such as distribution of medicines to different parts of the body and in the development of medical equipments for cell separation [12]. Several researchers analyzed blood flow in the presence of magnetic field and reported some clinical applications for their studies [13–16]. Ramamurthy and Shankar [17] and Rathod et al. [18] mentioned that the presence of external magnetic field significantly affects the vascular systems. Mekheimer and Kot [19] studied the influence of magnetic field and Hall current in blood flow through constricted arteries. Thus, the investigation on the blood flow in arteries in the presence of magnetic field is important.

Blood behaves like a Newtonian fluid when it flows in larger diameter arteries at high shear rates; but, it exhibits remarkable non-Newtonian character when it flows through smaller diameter arteries at low shear rates [20–22]. It is well known that blood flow in narrow arteries is highly pulsatile and in this flow situation, blood is modelled by a non-Newtonian fluid [23]. Sankar and Lee [24] performed finite difference method (FDM) analysis to study the effects of magnetic field on blood flow through stenosed narrow arteries, treating blood as Casson fluid model. The pulsatile flow of Herschel-Bulkley (H–B) fluid for blood flow in stenosed arteries in the presence of magnetic field has not been investigated by any one so far.

Scott Blair [25] reports "the residual variation which is the sum of the squares of the deviations of the observed values of stress from the estimated values was lowest for H–B fluid when compared with that of Casson fluid model". Scott Blair and Spanner [26] propounded that the

Casson fluid model can be used to model blood when it flows in smaller diameter tubes at moderate shear rates $\gamma < 10/\sec$; whereas, H–B fluid model can be used to model blood when it flows at low shear rate of flow in very narrow arteries where the yield stress is high. Iida [27] found that the velocity profiles in the arterioles having diameter less than 100 μm are generally fairly explained by both fluid models; but, the velocity profiles in the arterioles whose diameters are less than 65 μm do not conform to the Casson model. However, it can still be explained by H–B fluid model. In view of the aforesaid arguments, it is appropriate to treat blood as Herschel-Bulkley (H-B) fluid model rather than Casson fluid model when it flows through narrow arteries at low shear rates. In this study, we have analyzed the pulsatile flow of blood through stenosed arteries in the presence of magnetic field, treating blood as H-B fluid model and also compared the present results with the results of Sankar and Lee [24] for Casson fluid model.

The structure of our paper is as follows. Section 2 models the problem mathematically and then simplifies the momentum and constitutive equations through coordinate transformation. The finite difference method is applied for solving the transformed initial boundary value problem in section 3. The finite difference scheme for velocity, flow rate, skin friction and longitudinal impedance are obtained in section 3. The effects of magnetic field, maximum depth of the stenosis, yield stress, power law index, amplitude of the flow and phase angle on the aforesaid flow quantities are discussed in section 4. The estimates of the percentage of increase in the skin friction and longitudinal impedance to flow due to the presence of the magnetic filed at discrete points in the axial direction are also computed in section 4. The main results are summarized in the concluding section 5.

## 2 Mathematical formulation

### 2.1 Geometry of the flow filed and governing equations

Consider an axially symmetric, laminar, unsteady (pulsatile) and fully developed uni-directional flow (in the axial direction $(\bar{z})$) of a non-Newtonian viscous incompressible fluid (blood) through a circular artery with an axisymmetric mild stenosis in the presence of uniform transverse magnetic field $(\mathbf{B_0})$. The non-Newtonian behaviour of blood is characterized by Herschel-Bulkley (H-B) fluid. Since, blood possesses the property of diamagnetic material when oxygenated and paramagnetic when deoxygenated, blood is treated as magnetic fluid [28]. Due to the presence of stenosis in the artery, the wall of the artery is assumed as rigid. The arterial segment under study is assumed to be long enough so that the entrance, end and special wall effects can be neglected. Cylindrical polar coordinate system $(\bar{r},\bar{\psi},\bar{z})$ is used to analyze the blood flow, where $\bar{r}$ and $\bar{z}$ are the variables taken in the radial and axial directions respectively and $\bar{\psi}$ is the azimuthal angle. The geometry of the arterial segment with mild constriction is shown in Fig. 1. The equations of continuity and momentum for the magnetohydrodynamic (MHD) flow are

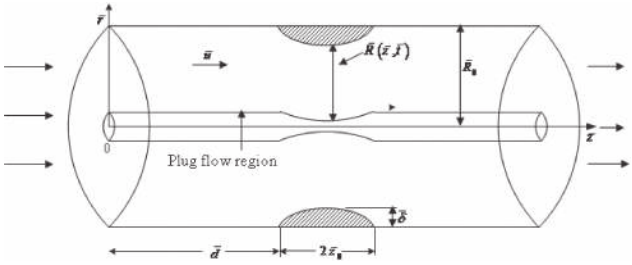


**Fig. 1:** Geometry of segment of an artery with axi-symmetric mild stenosis.

$$\nabla \bullet \mathbf{V} = 0 \tag{1}$$

$$\frac{D\mathbf{V}}{Dt} = -\frac{1}{\bar{\rho}}\nabla\bar{p} + \nabla \bullet \tau + \mathbf{J}\times\mathbf{B} \tag{2}$$

where $\mathbf{V}$ is the velocity vector, $D\mathbf{V}/Dt$ is the material derivative, $\bar{p}$ is the pressure, $\bar{\rho}$ is the density of the flowing fluid, $\tau$ is the stress tensor, $\mathbf{J}$ is the current density, $\mathbf{B}=\mathbf{B_0}+\mathbf{B_1}$ is the total magnetic field, $\mathbf{B_1}$ is the induced magnetic field which is assumed to be negligibly small when compared with the external magnetic field $B_0$ for MHD flow at small magnetic Reynolds number. The electric field due to the polarization of charge is also assumed as negligibly small. By Ohm's law, we have

$$\mathbf{J} = \sigma\left(\mathbf{E} + \mathbf{V}\times\mathbf{B}\right) \tag{3}$$

where $\sigma$ is the electrical conductivity and E is the electric field. The imposed and induced electrical fields are assumed to be negligible. Thus, the term $\mathbf{J}\times\mathbf{B}$ in Eq. (2) can be simplified as

$$\mathbf{J}\times\mathbf{B} = -\sigma\mathbf{B}^2\mathbf{V} \tag{4}$$

It can be shown that the radial velocity is negligibly small and can be neglected for a low Reynolds number flow. Since, the present study deal with the uni-directional

flow of blood in narrow arteries, the fluid-solid interaction between the flowing blood and the wall of the narrow artery is negligibly small in magnitude and can be ignored. However, this effect should be taken into consideration for two-dimensional flow of blood in large diameter arteries [29]. Thus, the momentum equations in the $\bar{z}$ and $\bar{r}$ directions in the presence of MHD interactions become

$$\bar{\rho}\frac{\partial \bar{u}}{\partial \bar{t}} = -\frac{\partial \bar{p}}{\partial \bar{z}} - \frac{1}{\bar{r}}\frac{\partial}{\partial \bar{r}}\left(\bar{r}\,\bar{\tau}\right) - \sigma B_0^2\,\bar{u} \tag{5}$$

$$0 = -\frac{\partial \bar{p}}{\partial \bar{r}} \tag{6}$$

where $\bar{\tau} = \bar{\tau}_{rz}$ is the shear stress. Since, the flow is assumed as slow, the magnitude of the inertial terms in the momentum equations are negligibly small and are neglected in Eqs. (5) and (6). The constitutive equation of the H-B fluid model which represents the blood when it flows in narrow arteries at low shear rates is

$$-\frac{\partial \bar{u}}{\partial \bar{r}} = \begin{cases} \dfrac{1}{\bar{\mu}_H}\left(\tau - \tau_y\right)^n & \text{if } \bar{\tau} \geq \bar{\tau}_y \\ 0 & \text{if } \tau \leq \tau_y \end{cases} \tag{7}$$

where $\bar{\tau}_y$ and $\bar{\mu}_H$ are the yield stress and viscosity of the H-B fluid respectively. Eq. (7) indicates that normal flow occurs in the region where the shear stress is greater than the yield stress of the fluid and plug flow (solid-like flow) occurs in the region where the shear stress is less than or equal to the yield stress of the fluid. Resolving Eq. (7) for the shear stress $\bar{\tau}$ and then substituting it in Eq. (5), we get

$$\frac{\partial \bar{u}}{\partial \bar{t}} = -\frac{1}{\bar{\rho}}\frac{\partial \bar{p}}{\partial \bar{z}} - \frac{1}{\bar{\rho}\,\bar{r}}\frac{\partial}{\partial \bar{r}}\left[\bar{r}\left(\tau_y + \left\{\mu_H\left(-\frac{\partial \bar{u}}{\partial \bar{r}}\right)\right\}^{1/n}\right)\right] - \frac{\sigma B_0^2\,\bar{u}}{\bar{\rho}} \tag{8}$$

Blood is transported into different parts of the body by means of the pressure gradient produced by the pumping action of the heart which is pulsatile in nature. The pressure gradient term in the momentum equation characterizes the pulsatile flow nature of blood flow. Hence, it is quite common to assume the pressure gradient term in the momentum equation (8) as the sum of the constant pressure gradient $A_0$ (for steady flow) and pulsatile pressure gradient $A_1$ (for unsteady flow) multiplied by a cosine function of the product of angular frequency and time as given below [16, 30].

$$-\frac{\partial \bar{p}}{\partial \bar{z}} = \bar{A}_0 + \bar{A}_1 \cos \bar{\omega}\,\bar{t} \tag{9}$$

where $\bar{\omega} = 2\pi\,\bar{f}$, $\bar{f}$ is the heart pulse rate. The geometry of the arterial segment with time dependent mild stenosis is defined by

$$\bar{R}\left(\bar{z},\bar{t}\right) = \begin{cases} \left[\bar{R}_0 - \dfrac{\bar{\delta}}{2}\left(1+\cos\left[\pi\left(\bar{z}-\bar{z}_1\right)/\bar{z}_0\right]\right)\right]a\left(\bar{t}\right) & \text{if } \bar{d} \leq \bar{z} \leq \bar{d} + 2\bar{z}_0 \\ \bar{R}_0\,a\left(\bar{t}\right) & \text{in the non-stenotic region} \end{cases} \tag{10}$$

where $\bar{R}\left(\bar{z},\,\bar{t}\right)$ is the radius of the arterial segment in the constricted part of the artery, $\bar{R}_0$ is the radius of the artery in the normal region, $\bar{z}_0$ is the semi-length of the stenosis, $\bar{z}_1$ is the centre of the stenosis and $\bar{\delta}$ is the maximum depth of the stenosis. The time-dependent parameter $\bar{a}\left(\bar{t}\right)$ is defined by

$$\bar{a}\left(\bar{t}\right) = 1 - k\cos\left(\bar{\omega}\bar{t} - \phi\right) \tag{11}$$

where $\phi$ is the phase angle, $k$ is the amplitude parameter.

## 2.2 Non-dimensionalization

Let us introduce the following non-dimensional variables.

$$r = \frac{\bar{r}}{\bar{R}_0},\ R = \frac{\bar{R}}{\bar{R}_0},\ z = \frac{\bar{z}}{\bar{R}_0},\ u = \frac{\bar{u}}{\left(\rho\bar{U}^2\bar{R}_0\right)/\mu_0},\ t = \frac{\bar{t}\,\bar{U}}{\bar{R}_0},\ p = \frac{\bar{p}}{\bar{\rho}\bar{U}^2},$$
$$\omega = \frac{\bar{\omega}\bar{R}_0}{\bar{U}},\ A_0 = \frac{\bar{R}_0\bar{A}_0}{\bar{\rho}\bar{U}^2},\ A_1 = \frac{\bar{R}_0\bar{A}_1}{\bar{\rho}\bar{U}^2},\ \delta = \frac{\bar{\delta}}{\bar{R}_0},\ \theta = \frac{\bar{\tau}_y}{\bar{\rho}\bar{U}^2},$$
$$\mathrm{Re} = \frac{\bar{\rho}\bar{U}\bar{R}_0}{\bar{\mu}_0},\ H = \frac{B_0\bar{R}_0\sqrt{\sigma}}{\sqrt{\bar{\mu}_0}} \tag{12}$$

where $\bar{\mu}_0 = \bar{\mu}_H\left(1/\bar{\rho}\bar{U}^2\bar{R}\right)$ has the dimension as that of Newtonian fluid's viscosity, *Re* is the Reynolds number and *H* is the Hartmann number which is a non-dimensional number representing the effects of magnetic field. Applying the non-dimensional variables defined in Eq. (12) into Eqs. (8)–(11), we obtain the dimensionless form of these equations respectively as the following equations.

$$\frac{\partial u}{\partial t} = -\frac{1}{\mathrm{Re}}\left[\frac{\partial p}{\partial z} + \frac{1}{r}\frac{\partial}{\partial r}\left\{r\left(\theta + \left\{-\frac{\partial u}{\partial r}\right\}^{1/n}\right)\right\} + H^2 u\right] \tag{13}$$

$$-\frac{\partial p}{\partial z} = A_0 + A_1\cos\omega t \tag{14}$$

$$R(z,t) = \begin{cases} \left[1-\frac{\delta}{2}\left(1+\cos\left[\pi\left(z-z_1\right)/z_0\right]\right)\right]a(t) & \text{if } d \le z \le d+2z_0 \\ a(t) & \text{in the non-stenotic region} \end{cases} \quad (15)$$

$$a(t) = 1 - k\cos(\omega t - \phi) \quad (16)$$

The non-dimensional form of the appropriate initial and boundary conditions are [15, 16]

$$u(r,z,0) = \begin{cases} \left(\frac{A_0+A_1}{H^2}\right)\left\{1-\frac{I_0(Hr)}{I_0(H)}\right\} & \text{in the presence of magnetic field} \\ \left(\frac{A_0+A_1}{4}\right)\left(1-\left(\frac{r}{R}\right)^2\right) & \text{in the absence of magnetic field} \end{cases} \quad (17)$$

$$\frac{\partial u}{\partial r}(r,z,t) = 0 \quad \text{at } r = 0 \quad (18)$$

$$u(r,z,t) = 0 \quad \text{at } r = R \quad (19)$$

where $I_0$ is the modified Bessel function of first kind and of order zero.

### 2.3 Radial coordinate transformation

Applying the radial coordinate transformation $\xi = r/R(z,t)$ into the momentum equation (13), one can obtain

$$\frac{\partial u}{\partial t} = -\frac{1}{\mathrm{Re}}\left[\frac{\partial p}{\partial z} + \frac{\theta}{\xi R} + \frac{1}{\xi R^{1+1/n}}\left(-\frac{\partial u}{\partial \xi}\right)^{1/n} + \frac{1}{nR^{1+1/n}}\left(-\frac{\partial u}{\partial \xi}\right)^{1/n-1}\left(-\frac{\partial^2 u}{\partial r^2}\right) + H^2 u\right] \quad (20)$$

Under radial coordinate transformation, boundary and initial conditions (17)–(19) become

$$u(\xi,z,0) = \begin{cases} \left(\frac{A_0+A_1}{H^2}\right)\left\{1-\frac{I_0(H\xi R)}{I_0(H)}\right\} & \text{in the presence of magnetic field} \\ \left(\frac{A_0+A_1}{4}\right)\left(1-\xi^2\right) & \text{in the absence of magnetic field} \end{cases} \quad (21)$$

$$\frac{\partial u}{\partial \xi}(0,z,t) = 0 \quad (22)$$

$$u(1,z,t) = 0 \quad (23)$$

## 3 Finite difference method of solution

The finite difference method is a straight forward and an efficient method for solving the resulting nonlinear partial differential equation (20) with the initial and boundary conditions (21)–(23). The central difference formula is used to approximate the spatial derivatives and forward difference formula is used to approximate the time derivative and are given below.

$$\frac{\partial u}{\partial \xi} = \frac{(u)^k_{i,j+1} - (u)^k_{i,j-1}}{2\Delta\xi} = \left(u_{f\xi}\right)^k_{i,j} \quad (24)$$

$$\frac{\partial^2 u}{\partial \xi^2} = \frac{(u)^k_{i,j+1} - 2(u)^k_{i,j} + (u)^k_{i,j-1}}{(\Delta\xi)^2} = \left(u_{s\xi}\right)^k_{i,j} \quad (25)$$

$$\frac{\partial u}{\partial t} = \frac{(u)^{k+1}_{i,j} - (u)^k_{i,j}}{\Delta t} \quad (26)$$

where, $\xi_j = (j-1)\Delta\xi$, $j = 1,2,\ldots N+1$ such that $\xi_{N+1} = 1$; $z_i = (i-1)\Delta z$, $i = 1,2,\ldots M+1$; $t_k = (k-1)\Delta t$, $k = 1,2,\ldots$ for the entire arterial segment under consideration with $\Delta\xi$ and $\Delta z$ being the respective increments in the radial and axial directions and $\Delta t$ being the time increment. Applying Eqs. (24)–(26) into the Eq. (20), the finite difference scheme for the velocity field can be obtained as:

$$u^{k+1}_{i,j} = u^k_{i,j} - \frac{\Delta t}{\mathrm{Re}}\left[-\left(-\frac{\partial p}{\partial z}\right)^{k+1} + \frac{\theta}{R^k_i \xi_j} + \frac{1}{\xi_j\left(R^k_i\right)^{1+1/n}}\left\{-\left(u_{f\xi}\right)^k_{i,j}\right\}^{1/n} + \frac{1}{n\left(R^k_i\right)^{1+1/n}}\left\{-\left(u_{f\xi}\right)^k_{i,j}\right\}^{1/n-1}\left\{-\left(u_{s\xi}\right)^k_{i,j}\right\} + H^2 u^k_{i,j}\right] \quad (27)$$

Using Eqs. (24)–(26) in the initial and boundary conditions (21)–(23), one can get

$$u^1_{i,j} = \begin{cases} \left(\frac{A_0+A_1}{H^2}\right)\left\{1-\frac{I_0(H\xi_j R^1_i)}{I_0(H)}\right\} & \text{in the presence of magnetic field} \\ \left(\frac{A_0+A_1}{4}\right)\left(1-\left(\xi_j R^1_i\right)^2\right) & \text{in the absence of magnetic field} \end{cases} \quad (28)$$

$$u^k_{i,1} = u^k_{i,2} \quad (29)$$

$$u^k_{i,N+1} = 0 \quad (30)$$

Using the computed velocity distribution, one can obtain the following finite difference schemes for the wall

shear stress, flow rate and longitudinal impedance to flow.

$$\left(\tau_w\right)_i^k = \theta + \left[\frac{1}{\left(R_i^k\right)}\left\{-\left(u_{f\xi}\right)_{i,N}^k\right\}\right]^{1/n} \tag{31}$$

$$Q_i^k = 2\pi\left(R_i^k\right)^2\left[\int_0^{\beta}\xi_j\, u_{i,j}^k\, d\xi_j + \int_{\beta}^{1}\xi_j\, u_{i,j}^k\, d\xi_j\right] \tag{32}$$

$$\lambda_i^k = \left(-\frac{\partial p}{\partial z}\right)^k \Big/ Q_i^k \tag{33}$$

where $\beta$ is the plug core radius.

# 4 Numerical simulations of results and discussion

The objective of the present analysis is to bring out the effects of the magnetic field, power law index, phase angle, pressure gradient, yield stress and maximum depth of the stenosis on the physiologically important flow quantities such as velocity, flow rate, wall shear stress and longitudinal impedance to flow. Sankar and Lee [24] mathematically analyzed the MHD flow of blood in constricted narrow arteries, modelling blood as Casson fluid. In this article, we have theoretically investigated the MHD flow of blood in narrow arteries with mild constriction, treating blood as Herschel-Bulkley fluid model and compared the present results with the results of Sankar and Lee [24].

For the numerical simulation of various flow quantities and to validate the present results with the published results, the values (range) used for different parameters in this analysis [16] are given below.

$$d = z_0 = 7,\ z_1 = 14,\ \beta = 0.025,\ A_0 = 0.2A_1, \mathrm{Re} = 300, t = 50;\ {}_0$$
$$A_0\text{: } 0.2-0.8;\ k,\omega\text{: } 0.02-0.05;\ \phi\text{: } 0.2-0.5,\ H\text{: } 0-4;$$
$$\theta\text{: } 0-0.15;\ \delta\text{: } 0-0.25,\ t\text{: } 0-90$$

The flow region is discretized by taking the step size in the axial and radial directions as $\Delta z = 0.05$ and $\Delta\xi = 0.025$ respectively and the time step is chosen as $\Delta t = 0.0001$ for convergence of the solution to the fifth order [16].

## 4.1 Velocity distribution

Fig. 2 shows the velocity distribution for different fluid models and for different values of the Hartmann number

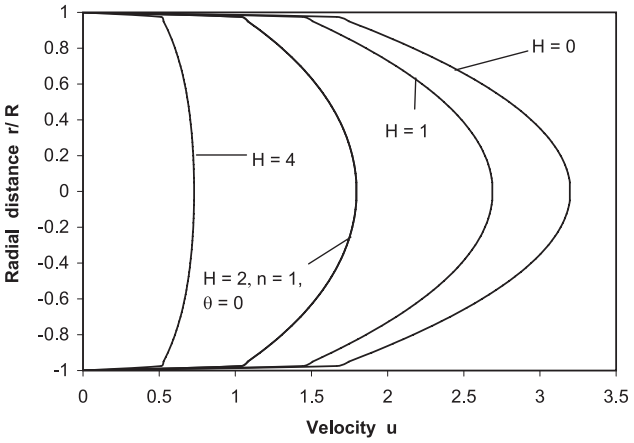


**Fig. 2:** Velocity distribution for different fluid models with $A_0 = 0.2$, $\omega = 0.02$, $k = 0.05$, $\phi = 0.2$, $\theta = 0.1$, $\delta = 0.276$ and $z = 14$.

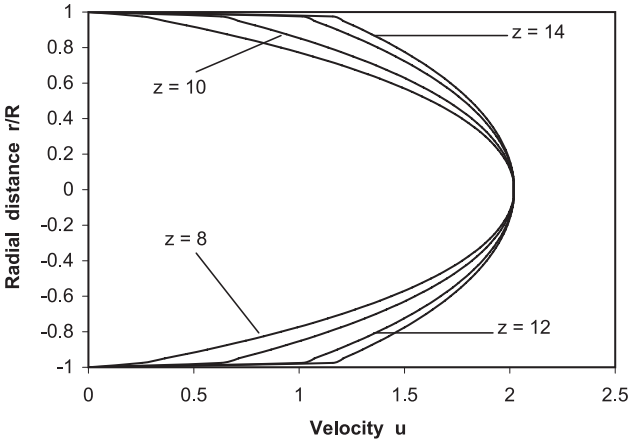


**Fig. 3:** Velocity distribution at different axial points with $n = 0.95$, $A_0 = 0.2$, $\omega = k = 0.02$, $\phi = 0.2$, $\theta = 0.1$, $\delta = 0.1$ and $H = 2$.

$H$ (parameter of the magnetic field) with $A_0 = 0.2$, $\omega = 0.02$, $k = 0.05$, $\phi = 0.2$, $\theta = 0.1$, $\delta = 0.276$ and $z = 14$. It is clear that the velocity decreases significantly with the increase of the Hartmann number $H$. i.e. the presence of magnetic field influences the velocity field by decreasing its magnitude significantly. It is also seen that for a given set of values of the parameters, the velocity of the H-B fluid model is significantly higher than that of the Casson fluid model. The plot of the velocity profile of the Newtonian fluid is in good agreement with that in Fig. 2 of Ikbal et al. [16].

The velocity distribution at discrete points in the axial direction (since, the stenosis is assumed to be symmetric, we have taken the discrete points in the first half of the stenosis) with $A_0 = 0.2$, $n = 0.95$, $\omega = k = 0.02$, $\phi = 0.2$, $\theta = \delta = 0.1$ and $H = 2$ is sketched in Fig. 3. It is seen that the velocity increases marginally with the increase of the axial variable $z$ in the first half of the stenosis and this behaviour

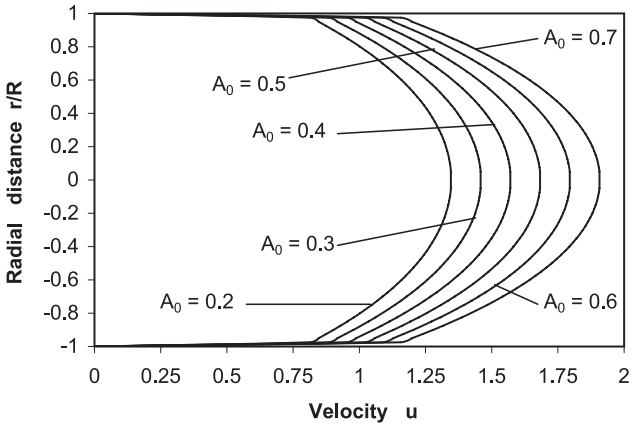


**Fig. 4:** Velocity distribution for different values of $A_0$ with $n = 0.95$, $H = 2$, $\omega = k = 0.02$, $\theta = \delta = 0.1$ and $\phi = 0.2$.

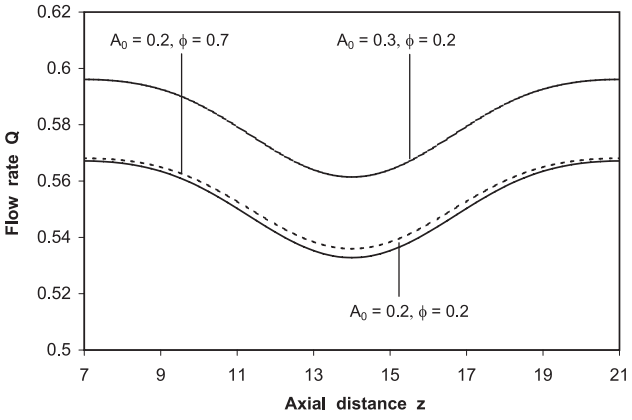


**Fig. 6:** Variation of flow rate with axial distance for different values of $A_0$ and $\phi$ with $H = 2$, $\omega = k = 0.02$, $n = 0.95$ and $\theta = \delta = 0.1$.

is expected to be reversed in the second half of the stenosis (not shown in the figure).

Fig. 4 shows the velocity distribution for different values of constant amplitude of the flow with $H = 2$, $n = 0.95$, $\omega = k = 0.02$, $\theta = \delta = 0.1$ and $\phi = 0.2$. The velocity distribution increases considerably with the increase of the amplitude of the flow when all the other parameters held constant. Figs. 2–4 bring out the effects of magnetic filed, amplitude of the flow and yield stress on the velocity distribution of blood when it flows in stenosed arteries.

## 4.2 Flow rate

The variation of flow rate with amplitude of the artery radius $k$ for different values of the Hartmann number $H$ with $n = 0.95$, $A_0 = 0.2$, $\omega = 0.02$, $\phi = 0.2$, $\theta = \delta = 0.1$ and $z = 14$ is sketched in Fig. 5. It is seen that the flow rate decreases slowly with the increase of the parameter $k$ from 0 to 0.02 and then it decreases rapidly (nonlinearly) with the increase of the parameter $k$ from 0.02 to 0.08. It is also observed that the flow rate decreases significantly with the increase of the Hartmann number $H$. (i.e. the presence of the magnetic field affects the flow rate by decreasing its magnitude significantly).

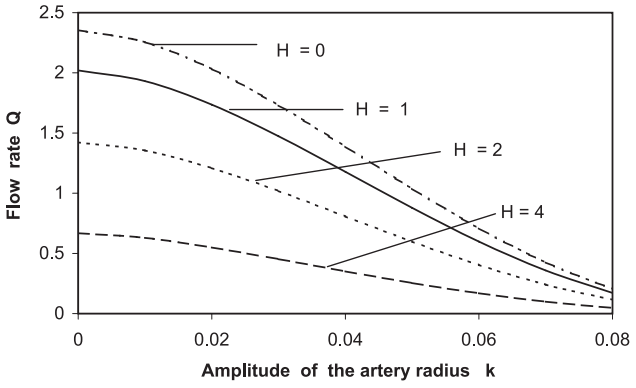


**Fig. 5:** Variation of flow rate with amplitude of the artery radius for different values of the Hartmann number $H$ with $n = 0.95$, $A_0 = 0.2$, $\omega = 0.02$, $\phi = 0.2$, $\theta = \delta = 0.1$ and $z = 14$.

Fig. 6 illustrates the variation of flow rate with axial distance for different values of the constant amplitude parameter $A_0$ and phase angle $\phi$ with $H = 2$, $\omega = k = 0.02$, $n = 0.95$ and $\theta = \delta = 0.1$. One can note that the flow rate decreases slowly with the increase of the axial variable $z$ from 7 to 9 and then it decreases quite fast as the axial variable $z$ increases from 9 to 14 and then it increases symmetrically as the axial variable $z$ increases further from 14 to 21. It is observed that for a given value of the phase angle $\phi$, the flow rate increases significantly with the increase of the amplitude of the flow. The flow rate increases slightly with the increase of the phase angle when the amplitude of the flow is kept as invariable. Figs. 5 and 6 exhibit the effects of magnetic filed, amplitude of the flow and phase angle on the flow rate of blood flow in stenosed arteries.

## 4.3 Skin friction

Skin friction is an important measurement in hemodynamics. Accurate prediction of skin friction distribution is useful in analyzing the effects of blood flow on the endothelial cells [31]. The variation of skin friction with axial distance for different fluid models with $A_0 = 0.5$, $\omega = 0.02$ and $\theta = \delta = 0.1$ is shown in Fig. 7. It is found that the skin friction increases slowly with the increase of the axial variable $z$ from 7 to 9 and then it increases considerably with the increase of '$z$' from 9 to 14 and, it decreases sig-

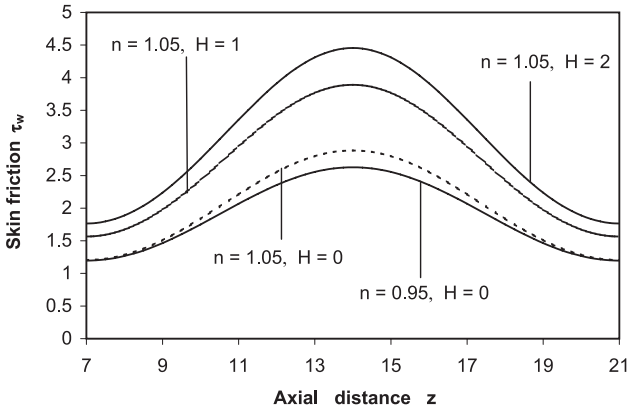


**Fig. 7:** Variation of skin friction with axial distance for Casson and H-B fluid models with $A_0 = 0.2$, $\omega = 0.02$ and $\theta = \delta = 0.1$.

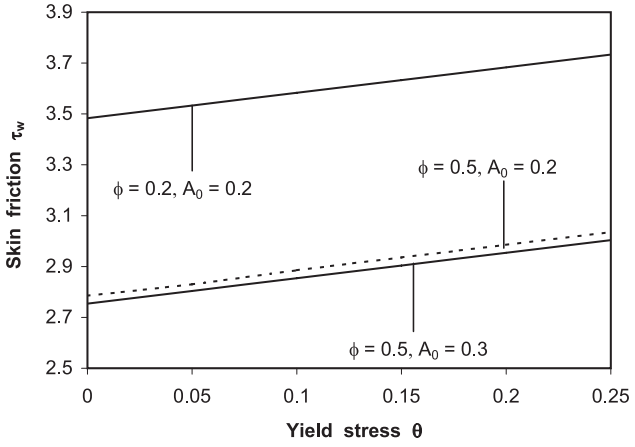


**Fig. 8:** Variation of skin friction with yield stress for different values of phase angle $\phi$ and constant pressure gradient $A_0$ with $n = 0.95$, $k = \omega = 0.02$ and $\theta = \delta = 0.1$.

nificantly with the increase of '$z$' from 14 to 19 and then it decreases slowly when '$z$' increases from 19 to 21. For a given value of the power law index $n$, the skin friction increases significantly with the increase of the Hartmann number $H$ which indicates that the presence of magnetic field influences the blood flow by increasing the skin friction. It is further observed that the skin friction increases marginally with the increase of the power law index when the Hartmann number is held fixed. Note that for a given set of values of the parameters, the skin friction is considerably lower for the H-B fluid model than that of the Casson fluid model.

Fig. 8 depicts the variation of skin friction with yield stress for different values of the phase angle $\phi$ and constant amplitude $A_0$ of the pressure gradient with $n = 0.95$, $\omega = k = 0.02$, $H = 2$, and $z = 14$. It is noticed that the skin friction increases linearly with the increase of the yield stress $\theta$. It is also clear that the skin friction decreases with the increase

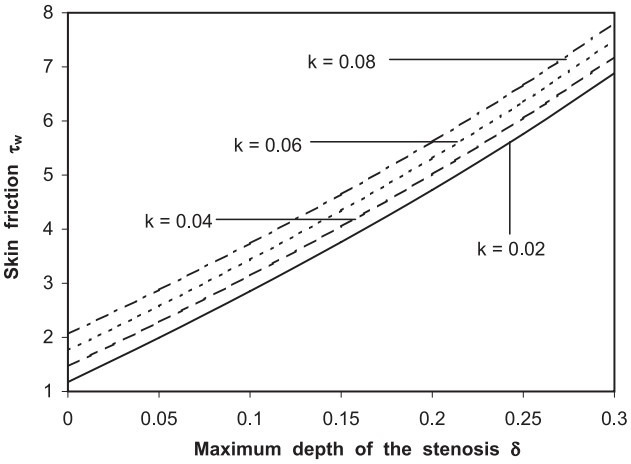


**Fig. 9:** Variation of skin friction with maximum depth of the stenosis for different values of the amplitude $k$ of the artery radius with $n = 0.95$, $\omega = 0.02$ and $\theta = 0.1$.

of either the phase angle $\phi$ or amplitude of the pulsatile flow $A_0$. But, the decrease in the skin friction is marginal when the amplitude of the pulsatile flow increases and is very significant when the phase angle increases.

The variation of skin friction with the maximum depth of the stenosis $\delta$ for different values of the amplitude parameter $k$ of the artery radius with $n = 0.95$, $H = 2$, $\omega = 0.02$ and $\theta = 0.1$ is shown in Fig. 9. It is clear that the skin friction increases linearly with the increase of the maximum depth of the stenosis. The skin friction increases marginally with the increase of the amplitude parameter $k$ of the artery radius. Figs. 6–9 spell out the effects of magnetic field, amplitude of flow, maximum depth of the stenosis, non-Newtonian behaviour of the flowing fluid and artery radius on the skin friction in the pulsatile flow of blood through a narrow artery.

## 4.4 Longitudinal impedance to flow

Fig. 10 shows the variation of longitudinal impedance to blood flow with the maximum depth of the stenosis for different values of the Hartmann number $H$ and the amplitude $k$ of the artery radius with $\omega = 0.02$, $\phi = 0.2$, $A_0 = 0.5$, $\delta = \theta = 0.1$ and $z = 14$. The longitudinal impedance to the flow increases very slowly with the increase of the maximum depth of the stenosis $\delta$ for lower values of the Hartmann number ($H = 0$, 2) and increases slightly (non-linearly) with the increase of the maximum depth of the stenosis $\delta$ for higher value of the Hartmann number ($H = 4$). It is clear that for a given value of the amplitude $k$ of the artery radius, the longitudinal impedance to flow increases significantly with the increase of the Hartmann number $H$. It is also noticed that the longitudinal

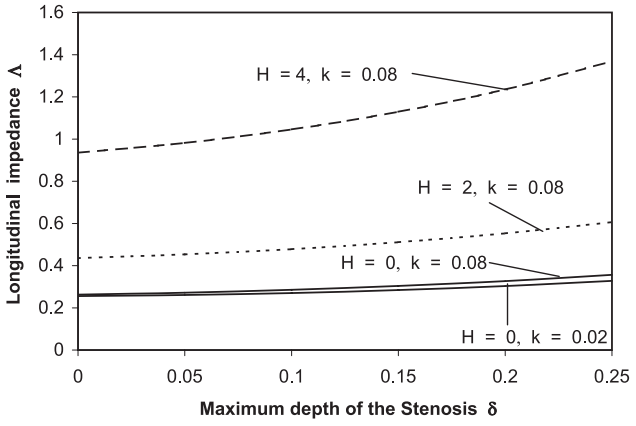


**Fig. 10:** Variation of longitudinal impedance to the flow with maximum depth of the stenosis for different values of $H$ and $k$ with $\omega = 0.02$, $\phi = 0.2$, $A_0 = 0.5$, $\theta = 0.1$ and $z = 14$.

impedance to flow increases slightly with the increase of the amplitude $k$ of the artery radius when the Hartmann number is held constant. Fig. 10 brings out the effects of the magnetic field, maximum depth of the stenosis and radius of the artery on the longitudinal impedance to blood flow.

## 4.5 Quantification of skin friction and longitudinal impedance

It is important to know the precise effects of the magnetic field in blood flow by quantifying the increase in the physiologically important flow measurements such as skin friction and longitudinal impedance to flow. The increase in the skin friction/longitudinal impedance to flow due to the presence of the magnetic field is defined as the ratio between the skin friction/longitudinal impedance of a fluid model in the presence of magnetic field for a given set of values of the parameters and the skin friction/longitudinal impedance of the same fluid in the absence of the magnetic field for the same set of values of the parameters.

The estimates of the increase in the skin friction for different values of the magnetic field parameter $H$ in the axial direction (upto the half of the stenosis length) for H-B fluid and Casson fluid [28] with $A_0 = 0.7$, $\theta = \delta = 0.1$, $k = \omega = 0.02$ and $\phi = 0.2$ are computed in Table 1. It is observed that estimates of the increase in the skin friction increase marginally with the increase of the axial variable '$z$' and increase significantly with the increase of the Hartmann number $H$. The estimates of the increase in the skin friction are considerably lower for H-B fluid model than those of the Casson fluid model.

The estimates of the increase in longitudinal impedance to flow are computed using the same procedure that was adopted for estimating the increase in the skin friction. The estimates of the increase in the longitudinal impedance to flow for different values of the Hartmann number $H$ in the axial direction for H-B fluid model and Casson fluid model with $A_0 = 0.7$, $k = \omega = 0.02$, $\theta = \delta = 0.1$ and $\phi = 0.2$ are given in Table 2. It is observed that the

**Table 1:** Estimates of the increase in skin friction due to the presence of magnetic field at discrete points in the axial direction for H-B and Casson fluid models with $A_0 = 0.7$, $\theta = \delta = 0.1$, $k = \omega = 0.02$ and $\phi = 0.2$.

| $z$ | | 7 | 8 | 9 | 10 | 11 | 12 | 13 | 14 |
|---|---|---|---|---|---|---|---|---|---|
| H-B fluid with $n = 0.95$ | H = 1 | 1.2926 | 1.2979 | 1.3118 | 1.3301 | 1.3489 | 1.3648 | 1.3753 | 1.3789 |
| | H = 2 | 1.7287 | 1.7422 | 1.7782 | 1.8263 | 1.8763 | 1.9192 | 1.9479 | 1.9580 |
| Casson fluid | H = 1 | 1.5937 | 1.6020 | 1.6244 | 1.6548 | 1.6868 | 1.7143 | 1.7329 | 1.7395 |
| | H = 2 | 2.0202 | 2.0359 | 2.0748 | 2.1289 | 2.1860 | 2.2357 | 2.2693 | 2.2811 |

**Table 2:** Estimates of the increase in longitudinal impedance due to the presence of magnetic field at discrete points in the axial direction for H-B and Casson fluid models with $A_0 = 0.7$, $k = \omega = 0.02$, $\theta = \delta = 0.1$ and $\phi = 0.2$.

| $z$ | | 7 | 8 | 9 | 10 | 11 | 12 | 13 | 14 |
|---|---|---|---|---|---|---|---|---|---|
| H-B fluid with $n = 0.95$ | H = 1 | 1.1633 | 1.1638 | 1.1644 | 1.1650 | 1.1656 | 1.1662 | 1.1669 | 1.1676 |
| | H = 2 | 1.6345 | 1.6385 | 1.6422 | 1.6465 | 1.6510 | 1.6558 | 1.6582 | 1.6621 |
| Casson fluid | H = 1 | 1.1659 | 1.1660 | 1.1662 | 1.1666 | 1.1671 | 1.1675 | 1.1679 | 1.1681 |
| | H = 2 | 1.6554 | 1.6556 | 1.6566 | 1.6584 | 1.6609 | 1.6635 | 1.6654 | 1.6662 |

estimates of the increase in the longitudinal impedance increase considerably with the increase of the Hartmann number $H$ and increase slightly with the increase of the axial variable '$z$'. It is also found that the estimates of the increase in the longitudinal impedance to flow are lower for the H-B fluid model than those of the Casson fluid model. It is important to mention that the presence of magnetic field influences the skin friction and longitudinal impedance of the flow by increasing their magnitude considerably.

## 5 Conclusion

The pulsatile flow of blood flow through narrow arteries with mild axi-symmetric stenosis in the presence of magnetic field is analyzed, treating blood as H-B fluid model. The main results of this study are summarized below:

- Velocity and flow rate decrease considerably and the skin friction and longitudinal impedance to flow increase significantly with the increase of the intensity of magnetic field parameter.
- Velocity of the H-B fluid model is significantly higher than that of the Casson fluid model.
- Flow rate increases and skin friction decreases with the increase of the pressure gradient.
- The longitudinal impedance to flow and skin friction increase with the increase of the amplitude $k$ of the artery radius.
- Skin friction and longitudinal impedance to flow increase with the increase of the maximum depth of the stenosis $\delta$.
- Estimates of the increase in the longitudinal impedance to flow and skin friction increase considerably with the increase of the intensity of the magnetic field.
- Estimates of the increase in the longitudinal impedance to flow and skin friction are considerably lower for H-B fluid model than those of the Casson fluid model.

The primary contribution of this study is the investigation on the MHD flow of Herschel-Bulkley fluid for blood flow in narrow arteries with mild constriction and this work is the complement to the study by Sankar and Lee [24] for the MHD flow of Casson fluid model for blood flow in constricted arteries. As the Herschel-Bulkley fluid model has many advantageous over Casson fluid model for blood flow modelling which are mentioned in the introduction section of this article, it is hoped that the present study may be considered as an improvement over the study of Sankar and Lee [24] and this mathematical model may be used to predict the physiologically important flow quantities which may find applications in the clinical case studies.

**Acknowledgments:** The present work was supported by the research university grant of Universiti Sains Malaysia, Malaysia (Grant Ref. No: 1001/PMATHS/811177) and by the Inha University Research Grant.

Received: June 4, 2012. Accepted: April 22, 2013.

## References

[1] S. Chakravarty, P. K. Mandal, A non-linear two-dimensional model of blood flow in an overlapping arterial stenosis subjected to body acceleration, *Math. Comp. Model.* 24 (1996) 43–58.

[2] G. A. Johnson, H. S. Borovetz, J. L. Anderson, A model of pulsatile flow in uniform deformable vessel, *J. Biomech.* 25 (1992) 91–100.

[3] S. Chakravarty, P. K. Mandal, Two-dimensional blood flows through tapered arteries under stenosed conditions, *Int. J. Non-Linear Mech.* 35 (2000) 779–793.

[4] K. S. Mekheimer, M. A. Kot, Suspension model for blood flow through arterial catheterization, *Chem. Eng. Comm.* 197 (2010) 1195–1214.

[5] R. Ponnalagusamy, Blood flow through an artery with mild stenosis: A two-layered model, different shapes of stenosis and slip velocity at the wall, *J. Appl. Sci.* 7 (2007) 1071–1077.

[6] D. Philip, P. Chandra, Flow of Eringen fluid (simple micro fluid) through an artery with mild stenosis, *Int. J. Eng. Sci.* 34 (1996) 87–99.

[7] I. Marshall, S. Zhao, P. Papathanasopoulou, P. Hoskins, X. Y. Xu, MRI and CFD studies of pulsatile flow in healthy and stenosed carotid bifurcation models, *J. Biomech.* 37 (2004) 679–687.

[8] K. S. Mekheimer, M. A. Kot, The micropolar fluid model for blood flow through a tapered stenotic arteries, *Acta Mechanica Sinica* 24 (2008) 637–644.

[9] N. Mushtapha, N. Amin, S. Chakravarty, P. K. Mandal, Unsteady magnetohydro-dynamic blood flow through irregular muti-stenosed arteries, *Comput. Biology Medicine* 39 (2009) 896–906.

[10] C. Midya, G. C. Layek, A. S. Gupta, M. T. Roy, Magenetohydrodynamic viscous flow separation in a channel with constrictions, *ASME J. Fluid Eng.* 125 (2009) 952–962.

[11] T. Higashi, A. Yamagishi, T. Takeuchi, N. Kawaguchi, S. Sagawa, M. Date, Orientation of erythrocytes in a strong magnetic field, *J. Blood* 82 (1993) 1328–1334.

[12] P. A. Voltairas, D. I. Fotiadis, L. K. Michalis, Hydrodynamics of magnetic drug targeting, *J. Biomech.* 35 (2002) 813–821.

[13] M. A. Ikbal, S. Chakravarty, K. L. Kelvin Wong, J. Mazumdar, P. K. Mandal, Unsteady response of non-Newtonian blood flow through a stenosed artery in magnetic field, *J. Computat. Appl. Math* 230 (2009) 243–259.

[14] M. Motta, Y. Haik, A. Gandhari, C. J. Chen, High magnetic field effects on human deoxygenated hemoglobin light absorption, *Bioelectrochem. Bioenerg.* 47 (1998) 297–300.
[15] A. R. Rao, K. S. Deshikachar, MHD oscillatory flow of blood through channels of variable cross section, *Int. J. Eng. Sci.* 24 (1986) 1915–1628.
[16] E. F. El-Shehawey, E. M. E. Elbarbary, N. A. S. Afifi, M. Elshahed, MHD flow of an elastico-viscous fluid under periodic body acceleration, *J. Math. Math. Sci.* 23 (2000) 795–799.
[17] G. Ramamurthy, B. Shankar, Magetohydrodynamics effects on blood flow through a porous channel, *Med. Biol. Eng. Computat.* 32 (1994) 655–659.
[18] V. P. Rathod, S. Tanveer, I. S. Rani, G. G. Rajput, Pulsatile flow of blood with periodic body acceleration and magnetic field through an exponentially diverging vessel, *Ultra Sci. Phys. Sci.* 18 (2006) 417–426.
[19] K. S. Mekheimer, M. A. Kot, Influence of magnetic field and Hall currents on blood flow through a stenotic artery, *Appl. Math. Mech. – Eng. Ed.* 29 (2008) 1093–1104.
[20] D. S. Sankar, Two-fluid nonlinear mathematical model for pulsatile blood flow through stenosed arteries, *Bull. Malays. Math. Sci. Soc.* 35 (2012) (2A) 487–495.
[21] R. K. Dash, G. Jayaraman, K. N. Metha, Estimation of increased flow resistance in a narrow catheterized artery – A theoretical model, *J. Biomech.* 29 (1996) 917–930.
[22] D. S. Sankar, U. Lee, Two-phase non-linear model for the flow through stenosed blood vessels, *J. Mech. Sci. Tech.* 21 (2007) 678–689.
[23] V. P. Rathod, S. Tanveer, Pulsatile flow of couple stress fluid through a porous medium with periodic body acceleration and magnetic field, *Bull. Malays. Math. Sci. Soc.* 32 (2) (2009) 245–259.
[24] D. S. Sankar, U. Lee, FDM analysis for MHD flow of a non-Newtonian fluid for blood flow in stenosed arteries, *J. Mech. Sci. Tech.* 25 (2011) 2573–2581.
[25] G. W. Scott Blair, The success of Casson equation, Rheologica Acta 5 (1966) 84–187.
[26] G. W. Scott Blair, D. C. Spanner, *An introduction to Biorheology,* Elsevier Scientific Publishing Company, Amsterdam, p. 51, 1974.
[27] N. Iida, Influence of plasma layer on steady blood flow in microvessels, *Japanese J. Appl. Phys.* 17 (1978) 203–214.
[28] Y. Haik, V. Pai, C. J. Chen, Biomagnetic fluid dynamics, in: W. Shyy, R. Narayanan (Eds.), *Fluid Dynamics at Interfaces,* Cambridge University Press, Cambridge, pp. 439–452, 1999.
[29] S. Z. Zhao, X. Y. Xu, M. W. Collins, The numerical analysis of fluid-solid interactions for blood flow in arterial structures, Part 2: Development of coupled solid-fluid algorithm, *Proceedings of the Institution of Mechanical Engineers, Part H: J. Eng. Medicine* 212 (1998) 241–252.
[30] S. Charavarty, P. K. Mandal, A. Mandal, Mathematical model of pulsatile blood flow in a distensible aortic bifurcation subject to body acceleration, *Int. J. Eng. Sci.* 38 (2000) 215–238.
[31] T. Karino, H. L. Goldsmith, Flow behaviour of blood cells and rigid spheres in annular vortex, *Philosophical Transactions Royal Society, London* B279 (1977) 413–445.